International Forum on Aeroelasticity and Structural Dynamics
IFASD 2024
17-21 June 2024, The Hague, The Netherlands

LIDAR-BASED GUST LOAD ALLEVIATION - INCREASING THE LOAD REDUCTION POTENTIAL THROUGH A TWO-DEGREE-OF-FREEDOM CONTROLLER ARCHITECTURE

Christian Wallace[1] **and Nicolas Fezans**[1]

[1] DLR (German Aerospace Center)
Institute of Flight Systems
Lilienthalplatz 7, 38108 Braunschweig, Germany
christian.wallace@dlr.de
nicolas.fezans@dlr.de

Keywords: Two-degree-of-freedom controller, gust load alleviation, lidar

Abstract: This paper proposes a two-degree-of-freedom (2-DoF) gust load alleviation (GLA) control architecture. Each "degree of freedom" was developed independently, either solely for load reduction purposes (in the case of the feedforward GLA part) or as a combination of a basic control law (load factor/C* normal law) and a feedback GLA control law. The basic control law influences the structural gust loads, even if not directly intended. The feedforward GLA part consists of a lidar-based controller, using wind field measurements ahead of the aircraft. To prevent unnecessarily aggressive controller commands for flight points at which lower load alleviation levels are required, the gains of the feedforward GLA control law and the gains of the feedback GLA control law are both scheduled via the true airspeed. Furthermore, a precompensation term is included to prevent the feedback laws (basic control law and GLA) from fighting the feedforward GLA commands. This precompensation works through the use of a reduced-order prediction model and additional connections from the feedforward GLA controller to the inputs of the feedback controllers. In a sense, the prediction model and the connections allow the feedforward GLA controller to "inform" the feedback controllers of its intentions. The load alleviation performance is evaluated on a representative hybrid (continuous and multi-rate discrete time) environment for a wide range of mass cases, flight points, and gust lengths, leading to results based on 864 different load cases. The proposed control architecture yields a reduction in peak bending moment of about 23 % in the area between the important wing root and the engine pylon, and still over 10 % near the wing tip.

1 INTRODUCTION

Aeroplanes in operational service are inevitably exposed to manifold structural loads. Besides the landing and manoeuvring loads, the aeroplane is also subject to external disturbances like turbulence and gusts. Active gust load alleviation provides the opportunity to exploit potentials to modify and redistribute the wing lift distribution to lower structural loads dynamically. Alleviated structural gust loads enable to design a potentially lighter structure, and the decreased aircraft net weight reduces the required amount of lift, correspondingly to the induced drag, and, therefore, the fuel consumption.

Active alleviation of gust loads is challenging and quite strongly limited by the available reaction time for the controller, considering the sensing of the gust or of its effect on the structure,

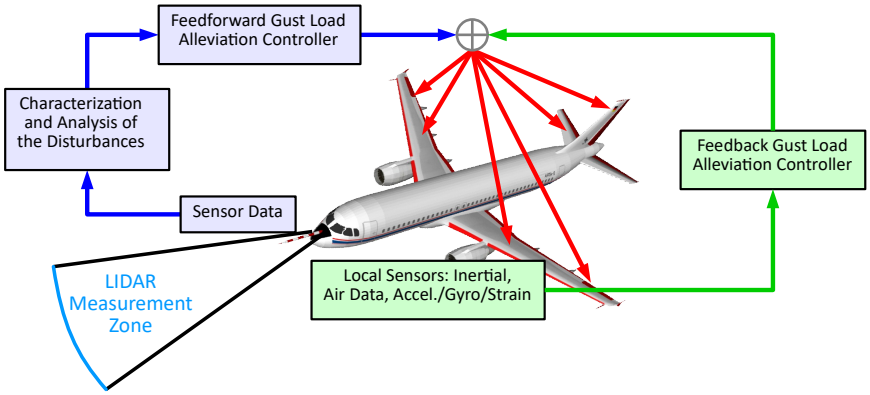

Figure 1: Schematic Illustration of Combined Lidar-based Feedforward and Feedback GLA Control [1]

delays in the loop, the actuator bandwidth and rate limiters. Being able to sense the gust slightly in advance, typically 0.2 to 0.6 seconds before encountering it, drastically increases the reachable level of gust load alleviation [2, 3]. Such anticipation could become possible with Doppler wind lidar sensors. A measurement zone ahead of the aeroplane is scanned permanently (Figure 1) by the lidar sensor. The resulting measurements are relative velocities between the sensor and molecules of the air in the so-called line-of-sight direction (laser beam axis), which need to be combined to estimate the vertical wind ahead of the aircraft. The latter is done with a so-called wind reconstruction algorithm.

In recent years, various aspects linked to lidar-based gust load alleviation systems have been investigated by the authors as well as their research group and partners, see [4] and references therein. The work performed includes investigation on the processing of lidar sensor measurements [3, 5, 6] and sensitivity studies to determine the required performance, accuracy, etc. for use in feedforward gust load alleviation [5] as well as the optimal tuning of the wind reconstruction algorithm used [5]. Various aspects related to the optimal tuning of such lidar-based gust load alleviation functions have been also investigated, see for instance [7] for the consideration of the wind estimation performance directly in the controller synthesis, [8] and references therein for the overall tuning methodology, or [9] for the multi-fidelity assessment strategies of complex active gust load alleviation architectures.

After the above-mentioned topics of gust load alleviation have been investigated in recent years, the integration of lidar-based feedforward GLA controllers into larger controller structures has (once again) become a focus of research for the authors. In practice, and as proposed in this paper, a feedforward gust load alleviation control function would have to be combined with other control functions, such as baseline controllers (e.g. manual control laws, autopilot functions) and feedback gust load alleviation controllers [1, 10]. The integration of independently designed controller functions, in particular, poses a number of challenges. Lidar-based vertical wind estimates enable feedforward gust load alleviation (GLA) control functions to start taking control actions before changes in the aerodynamic loads occur. A key challenge in this regard is that the pitching motion that the feedforward GLA control function (1-DoF) would typically command before encountering the gust, could be seen as a deviation of the desired state by the feedback control functions (1-DoF), but they should not counteract it. Since this problem has already been addressed in [11], this paper aims to propose a solution for integrating (lidar-based) feedforward GLA controller functions into multi-functional (feedback-) controller structures, avoiding counteracting controller activities.

The central element of the proposed solution is a feedforward GLA controller, which is augmented with a so-called prediction model. The prediction model represents, as a significantly

reduced-order model, the essential dynamics of the aircraft. When applying the feedforward GLA control commands also to the prediction model, its output can be inverted and superposed with the measurement signals used by the feedback controller(s). The intended influence of the feedforward GLA control law on the aircraft is, therefore, (barely) present for the feedback controllers. This enables an increase in the level of load alleviation achieved by superimposing the performance of the individual controller functions. Taking the proposed mechanism into account, this paper focuses on the design and application of a new 2-DoF-controller structure, applied to a twin-engine generic long-range aircraft configuration, which is representative of an industry-size load alleviation control design problem. The considered aircraft configuration was already part of an in-depth gust load analysis, investigating the impact of lidar-based feedforward GLA control on a wide range of mass distributions and flight points [12].

The remainder of this paper is structured as follows: Section 2 describes the considered application, the models, the main evaluation environment, the considered gust load cases and is concluded with a description of the open loop gust load behaviour. Section 3 presents the controller design methodologies, the tuning, the overall controller structure and the precompensation term. The latter includes the low-order prediction model and the interconnections between the feedforward GLA control law and the remaining controllers. Finally, sections 4 and 5, respectively, present the results and summary/outlook of this work.

2 AIRCRAFT CONFIGURATION AND EVALUATION ENVIRONMENT

This section presents the Generic Long Range Aircraft (GLRA) model that is considered in this work, the way the gust load envelope is defined and evaluated, and a discussion of the open-loop structural load results.

2.1 Considered Long-Range Aircraft Configuration

The Generic Long Range Aircraft (GLRA) is a wide-body twin-jet long-range research aircraft configuration. It features a classical wing (each wing is equipped with four independent ailerons) retrofitted with a large winglet (including an additional control surface called winglet tab) and downer and has an aspect ratio of about 9.5. Due to the need to use the GLRA for detailed flight simulations and/or as a realistic platform for controller development purposes, the configuration is represented by a detailed aeroelastic aircraft model composed by the DLR modelling approach called VarLoads [13].

VarLoads relies on the so-called “mean-axes formulation” [14]. This approach consists of nonlinear Newton-Euler equations of motion for the rigid body part, which are coupled with linear modal equations of motion for the structural dynamics part. Both the rigid and the elastic model parts are excited by propulsion and aerodynamic forces. The aerodynamic loads are derived by applying an unsteady panel method based on potential flow theory, namely the doublet lattice method (DLM). The DLM calculates the aerodynamic matrices at discrete reduced frequencies. A so-called rational function approximation (RFA) is used to use this data for time domain simulations, which allows the unsteady aerodynamic model to be cast in state space form. The cut loads are recovered by the so-called force summation method (FSM) [15].

In this work, similar to the application presented in [12], nine different mass distributions were available for the GLA controller development (Figure 2a), comprising a wide range of total masses and locations for the centre of gravity. The mass range varies between a lightweight mass case equivalent to the operational empty mass case (MOOee), and cases (MTFFJ, MTAAJ, and MTmMG) which are close or equivalent to the maximum take-off mass. The locations of

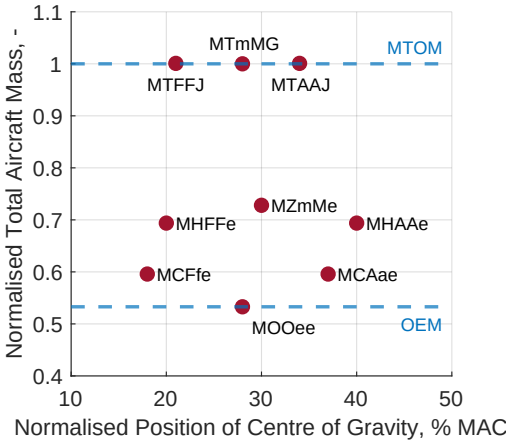

a) Normalised total aircraft mass vs. centre of gravity location.

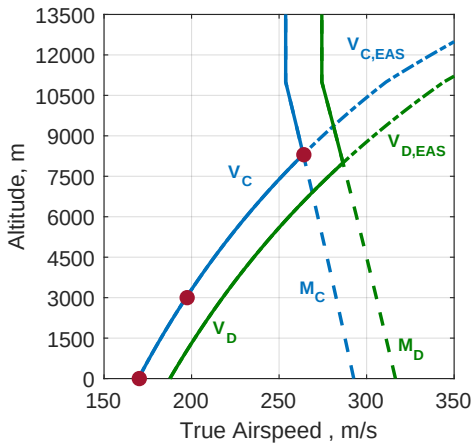

b) Reference design speeds. Cruise Mach number $M_C = 0.86$; Dive Mach number $M_D = 0.93$; Design cruise speed $V_{C,EAS} = 170.00$ m/s; Design dive speed $V_{D,EAS} = 188.00$ m/s.

Figure 2: Design Flight Points and Design Mass Cases for GLA Controller Development (red dots)

the centre of gravity vary between a more forward position (MCFfe, MHFFe, and MTFFJ) and a more rearward position (MCAae, MHAAe, and MTAAJ). The outlined modelling approach leads to an unique non-linear model for each mass case, which is trimmed afterwards at different flight points and linearised at the corresponding trim conditions. Based on a preliminary loads analysis, the selected flight points comprise three flight altitudes (0 m, 3000 m, and 8300 m), all considered at the specific design cruise speed V_C (according to the certification rule CS 25.335 [16]), and are represented with red dots in Figure 2b. For different flight altitudes, V_C corresponds to different true airspeeds and/or Mach numbers.

Table 1: Overview of Linear Aeroelastic Aircraft Models Available for GLA Controller Development

Mass Cases	**Design Flight Points**				**Trim Condition**	**Wing Conditions**
	Altitude	Design Speed	True Airspeed	Mach Number		
MCAae MCFfe MHAAe MHFFe MOOee MTAAJ MTFFJ MTmMG MZmMe	0.0 m	V_C	170.00 m/s	0.50	steady-horizontal-flight	clean, airbrake-out
	3000.0 m	V_C	197.34 m/s	0.60		
	8300.0 m	V_C	264.26 m/s	0.86		

In addition to *clean wing* conditions, *airbrake-out* cases are considered as well: for each combination of mass case and flight point, the same trim and linearisation process as for the *clean wing* configuration (i.e. only horizontal stabiliser deflection) is performed with constant $35°$ deflection of all spoilers. The difference between the *airbrake-out* and *clean wing* conditions is that the airbrakes reduce the total lift, which needs to be compensated by a higher angle of attack. This changes the lift distribution along the wing, the torsional moment along the wing, and, therefore, the flight shape. This also changes the local lift increases that a gust would induce

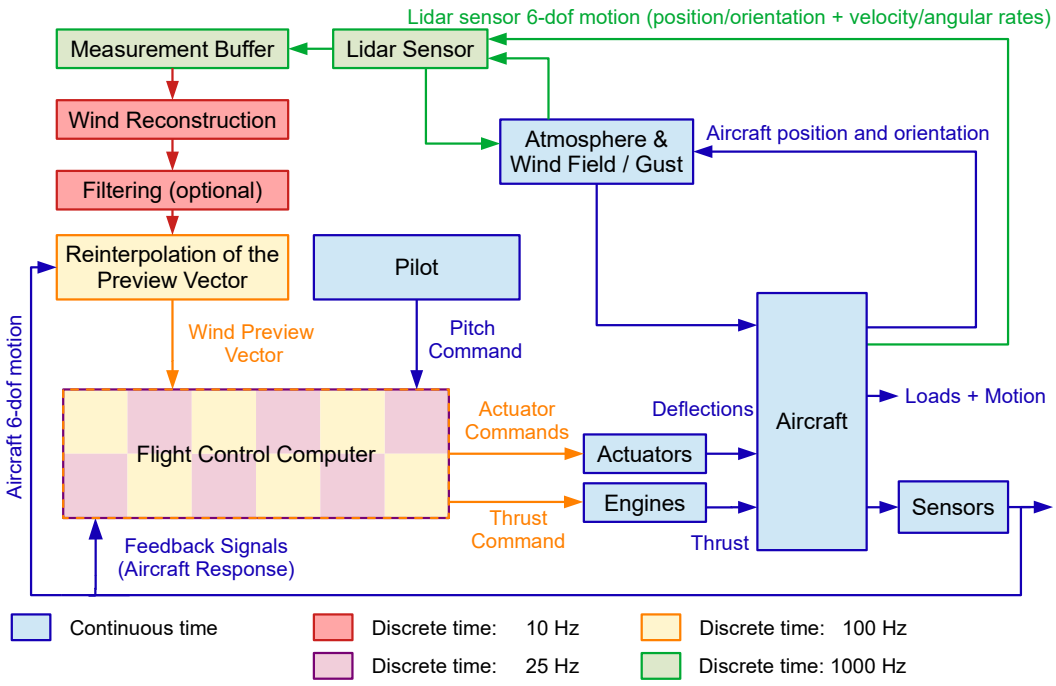

Figure 3: Overview of the Multi-Rate Hybrid Simulation of the Complete System

and so the dynamic response of the aircraft. Regarding active load alleviation, this also means that spoiler deflections cannot be used to reduce the gust loads when these spoilers are already fully deflected. Apart from worries that the use of dynamic spoiler deflections in the gust load alleviation function might lead to triggering buffeting effects, the fact that the peak gust load envelope is defined by *airbrake-out* cases for some parts of the wing motivated the investigation of the load alleviation potential when not using the spoilers for gust load alleviation.

Overall, 54 different aeroelastic models are available (Table 1). Each linear model provides flight mechanical parameters like position, velocities, angular rates, and air data parameters, which consists of the angle of attack and the angle of sideslip . Each linear model has 36 inputs for the control surfaces: i.a. eight different ailerons, two winglet tabs, six flaps, and 12 spoilers. The wind inputs are defined through 50 different planes distributed along and perpendicular to the fuselage axis. For each plane, the normalised vertical wind velocity (normalised by dividing it with the true airspeed) and its time derivative are required. This results in 100 wind inputs in total. The structural model contains over 400 distributed structural points to monitor cut loads, resulting in over 2500 cut load outputs (three forces and three moments for each point). Over 4800 outputs are used to display velocities and accelerations at various distributed locations on the flexible aircraft structure. Each linear aeroelastic state-space model has about 2800 states.

2.2 Simulation and Evaluation Environment

A realistic modular hybrid and multi-rate simulation environment [9] is used to simulate the various gust encounters and thereby assess the load alleviation performance. This environment is the most powerful and precise evaluation environment being available for the authors' for load alleviation controller development and assessment. It consists of MATLAB® and Simulink® components as well as C++ code. The numerical solvers provided with Simulink® allow the simulation of continuous-time, discrete-time, and hybrid[1] systems. Figure 3 illustrates the overall structure of the environment, as it is used in the present work. The continuous-time com-

[1] i.e. involving both continuous-time and discrete-time elements

ponents are represented by the light-blue blocks, and the discrete-time components are represented by the other colours (each colour represents a different rate). The environment consists of the linear aeroelastic aircraft model and actuator models, composing the aeroservoelastic sub-model, a lidar sensor simulation, an online wind reconstruction algorithm to interpret the lidar measurements, and the control functions. The different systems/functions run with the correct rate: the flight physics run in continuous time, the flight control computer with different partitions (25 Hz and 100 Hz), the wind reconstruction at 10 Hz, and the lidar at its own much faster rate (1 kHz).

To enhance the accuracy of the simulation, the Simulink®-based evaluation environment includes generic non-linear actuator models for each control surface. The generic non-linear actuator models are second-order systems with dynamically adjustable parameters (angular frequency, damping, gain) and with position, rate, and acceleration limits. These parameters can be adjusted: for each actuator independently, depending on the flight point, and asymmetrically (e.g. to account for aerodynamic and inertial loads acting on the control surface). In the present work, only the actuators for the elevators and the ailerons are controlled by the designed control functions. All controlled actuators are adjusted via the same fixed (irrespective of the current flight point) parameters (low-pass cut-off frequency of 4.875 Hz, a damping coefficient of 0.9, and a gain of 1.0). Specific non-linear limitations for the control surface positions and rates are implemented additionally, specifically defined for each corresponding control device group, as can be seen (as actuator drive-train limitations) in Table 2. The non-linear actuator drive-train limitations are the same for the entire flight envelope. Additionally, "GLA-specific Command Limitations" are implemented. They restrict the gust load alleviation authority directly in the flight control computer (as can be seen later in Figure 6). These limits apply to the sum of the commands of all active GLA-control functions.

Table 2: Implemented Non-Linear Control Device Command and Actuator Limitations

Control Surface Group	**GLA-specific Command Limitations**		**Actuator Drivetrain Limitations**	
	Deflection	Rate	Deflection	Rate
Elevators	$\pm 20°$	$\pm 50°$/s	$\pm 25°$	$\pm 50°$/s
Ailerons	$\pm 20°$	$\pm 50°$/s	$\pm 25°$	$\pm 50°$/s

In addition to the implemented actuator models, a sub-module for the engine dynamics is also foreseen to be part of the multi-rate hybrid simulation environment (Figure 3). Due to the investigated controller architecture, the engine model receives incremental thrust (lever) commands from the baseline controller in order to compensate for airspeed variations (as described later in Section 3.1). In this work, the engines are implemented as static dummy models without internal dynamics[2], so that resulting structural load variations are caused instantaneously by undelayed thrust (command) variations.

The multi-rate and hybrid simulation environment is furthermore equipped with a lidar-based wind estimation system that provides the so-called wind preview vector as a measured variable for the feedforward GLA controller. The system is based on a Doppler lidar and is capable of detecting relative wind speeds far away from the aircraft in the direction of flight. The combination of the lidar sensor, the scanning system and a wind estimation algorithm provides

[2]The used gain equals 1.

estimates of vertical wind speeds concerning the scanned area in front of the aircraft (Figure 1). The estimates of the vertical wind speeds are noisy and imperfect. The overall system is complex, the interested reader is referred therefore to older publications [4, 5, 7, 17]. The feedforward GLA controller (as a part of the FCC, Figure 3) receives a vertical wind profile as a vector of wind estimates along a portion of the flight path starting roughly at the aft of the aircraft and ending at the position that the aircraft reference point will have in h_{preview} time steps, which is schematically illustrated in Figure 4.

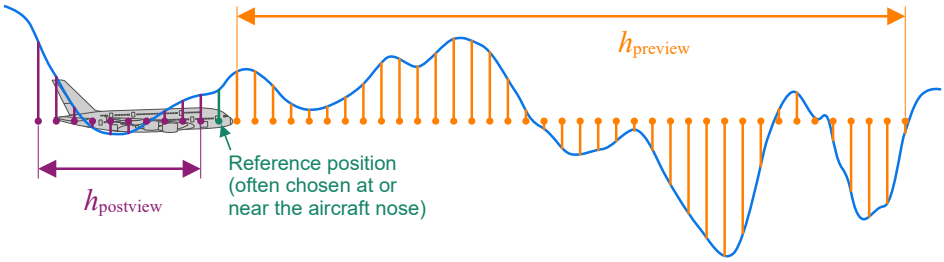

Figure 4: Preview and Postview Discretization of the Wind Field

Depending of the considered aircraft, the values h_{postview} and h_{preview} need to be adapted to the size of the aircraft, the critical gust lengths, and the chosen reference position. The farthest point also need to be compatible with the measurement range of the lidar. In practice, with geometrical effects and the need to have a minimum number of measurements performed around the farthest locations considered to obtain a sufficiently precise estimate of the vertical wind, the farthest point considered in the preview vector used by the controller is not as far as the farthest measurements performed by the lidar sensor. In the considered application, the farthest points measured by the lidar sensor were always (i.e. for all flight points) at about 182 m ahead of the aircraft nose. In contrast, the farthest point considered in the preview vector was only at about 148 m ahead of the aircraft nose. This corresponds to at least 0.560 s when flying at the maximum true airspeed value of 264.26 m/s of the considered flight points. As the feedforward GLA controller is discretised with a sampling time of 10 ms (as can be seen later in Subsection 3.3), this corresponds to $h_{\text{preview}} = 56$ samples. To ensure that the entire aircraft geometry, i.e. from the reference point around the nose position up to the tail, is covered by the preview vector, h_{postview} was set to 26 samples. The size of the estimated wind vector as input of the feedforward GLA controller is then $n_{\text{inputs}} = h_{\text{preview}} + 1 + h_{\text{postview}} = 83$. This corresponds to the maximum available wind vector length that the feedforward GLA control function uses.

2.3 Considered Gust Load Cases

The simulated gust load cases are defined according to paragraph CS 25.341a [16]. To ensure a detailed evaluation of the controlled aircraft behaviour in comparison to the open-loop aircraft behaviour, a representative set of gust load cases was chosen for analysis. The chosen set of gust load cases consists of symmetrical gusts with eight different gust lengths. Symmetrical gusts are characterised by a constant wind velocity over the complete wingspan. The gust lengths are distributed equidistantly between 9 m and 107 m. All gust lengths are simulated twice as an upward and a downward gust separately. 16 different gust load cases are simulated per linear model, leading to 864 gust load cases per controller configuration (respectively, the open-loop case). Hence, both the performance analysis of an individual controller function as well as an entire controller configuration (which consists of several controller functions activated in parallel) are based on exploiting symmetrical load cases (wings level, no sideslip, no lateral gust) solely. Therefore, it is assumed to be sufficient to illustrate only results for the right side of the aircraft (e.g. load stations of the right wing) to discuss the structural behaviour in detail.

2.4 Structural Loads Distribution without Control

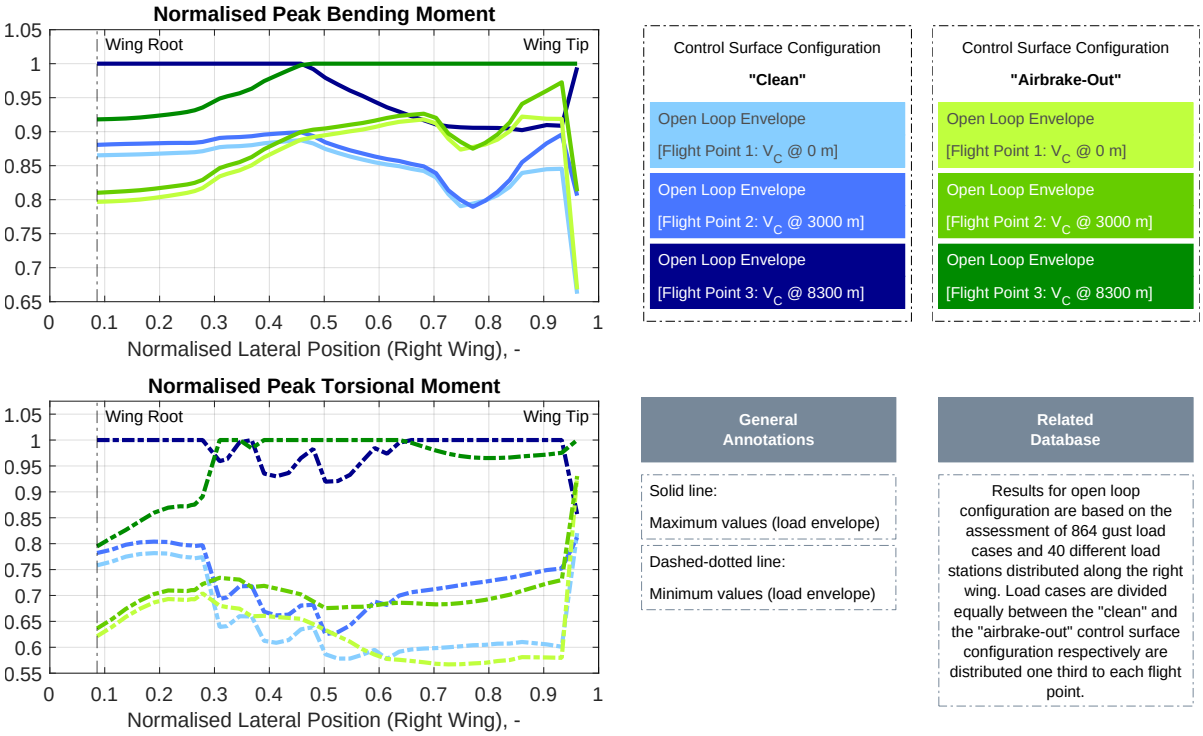

Figure 5: Distribution of Structural Peak Loads shown for the Aircraft Wing, without Active Load Control and broken down by Flight Points and Control Surface Configurations

The knowledge of the structural load behaviour of an uncontrolled aircraft is the initial starting point for the design process of load alleviation controllers. The GLRA aircraft model enables to evaluate structural loads on the entire structure. Gust loads can be determined for each single load case, each structural point and each load type, enabling to illustrate multiple load case hierarchies and load envelopes. Load case hierarchies are used to identify the most critical gust load cases and, as in this investigation, the responsible linear aircraft models. In the present work, the main objective of active load alleviation is to to save aircraft net weight via lighten the wing primary structure. Without precise knowledge of the detailed structural design of the wings and structural load envelopes other than gust load envelopes (e.g. manoeuvre load envelopes), it is not possible to make an exact forecast of what type of load must be lowered at what load station and by what percentage to achieve the best possible structural mass reduction. Based on the authors' experience, the gust load alleviation controller design is based mainly on the assumption that the maximum bending moment at the wing root in particular and the distribution of the bending moment over the entire wingspan, in general, have both a decisive influence on the dimensioning of the wing structure. Hence, the main objective of the GLA controller design (discussed later in Subsection 3.5) is to maximise the reduction of bending loads on the wing, especially at the wing root. The torsional moment distribution on the wing is generally much smaller, so it has less influence on the dimensioning of the structure. The final design of the controller structure may lead to a slightly increased distribution of the torsional moment, but the latter should be minimised or avoided if possible.

Figure 5 presents the peak gust load distribution for the bending moment and the torsional moment along the (right) wingspan for the uncontrolled aircraft. Both load distributions are subdivided into multiple sub-envelopes. The chosen decomposition leads primarily to two sub-datasets, *clean-wing*-envelopes (recognisable as a set of blue lines) and *airbrake-out*-envelopes

(recognisable as a set of green lines), and secondarily to envelopes composed by flight point-dependent load cases (distinguishable by different shades of the same colour). Regarding the absolute distribution of the peak loads (not shown here), the positive values dominate in case of the bending moment and the negative values in case of the torsional moment, so that the representation of the normalised envelopes is limited to positive values for the bending moment distribution and negative values for the torsional moment distribution (this also applies to all subsequent shown illustrations relating to loads). Each normalised open-loop envelope is normalised using the full open-loop envelope (based on all 864 gust load cases, not shown here, equivalent to a constant line of value 1).

Regarding the distribution of the bending moments, maximum structural loads are generated by load cases simulated at flight point 3. The *clean*-load cases dominate up to about half of the wingspan, but then are replaced by the *airbrake-out*-load cases at the outer wing. This alternating peak load behaviour can also be observed locally for flight point 1 and flight point 2. Within both control surface configurations, the flight-point-dependent local envelopes can be arranged, in terms of the impact on the load hierarchy, in descending order from flight point 3 to flight point 1. Towards the wing tip, the non-sizing local *airbrake-out*-load envelopes of flight point 1 and flight point 2 comprise higher maximum structural loads than the *clean* control surface configuration of flight point 3. The distribution of the torsional moment shows almost the same characteristics, although there are two significant differences. The *airbrake-out*-load cases are not dominant in the outer area of the wing (across all available flight points), but rather approximately between the engine mounting and the positions of the ailerons. Furthermore, both the load envelopes of flight point 1 and flight point 2 of the *airbrake-out* control surface configuration do not become more dominant than the *clean*-load case envelope of flight point 3 (neglecting the outermost load station at the wing tip).

3 DESIGNING THE TWO-DEGREE-OF-FREEDOM CONTROLLER

The overall control concept of the 2-DoF controller structure (Figure 6) consists of feedback and feedforward control elements. The part for the gust load alleviation is composed by a feedforward GLA controller and a feedback GLA controller, whose commands are superposed and potentially limited by GLA-specific limitations for the control surface deflections and rates (Table 2). The overall controller structure is completed by a baseline control function, which consists (internally) of feedforward and feedback control elements. The gust load alleviation controllers provide only actuator commands, whereas the baseline controller provides commands for the elevator and additional thrust (lever) commands. The superposed and (potentially) limited gust load alleviation actuator commands are superposed with the baseline actuator commands. The resulting total commands are not subject to any additional limitation in the Flight Control Computer (FCC) and are provided to the actuator models. The inputs of both feedback controllers are superposed via additional signals provided by the feedforward GLA controller, precompensating the expected aircraft reaction due to the feedforward GLA commands. This innovative mechanism is particularly discussed in Subsection 3.3.2. In this section, the individual components of the controller structure, the design process for the gust load alleviation control functions, the corresponding optimisation criteria and the true airspeed-dependent gain scheduling are described below.

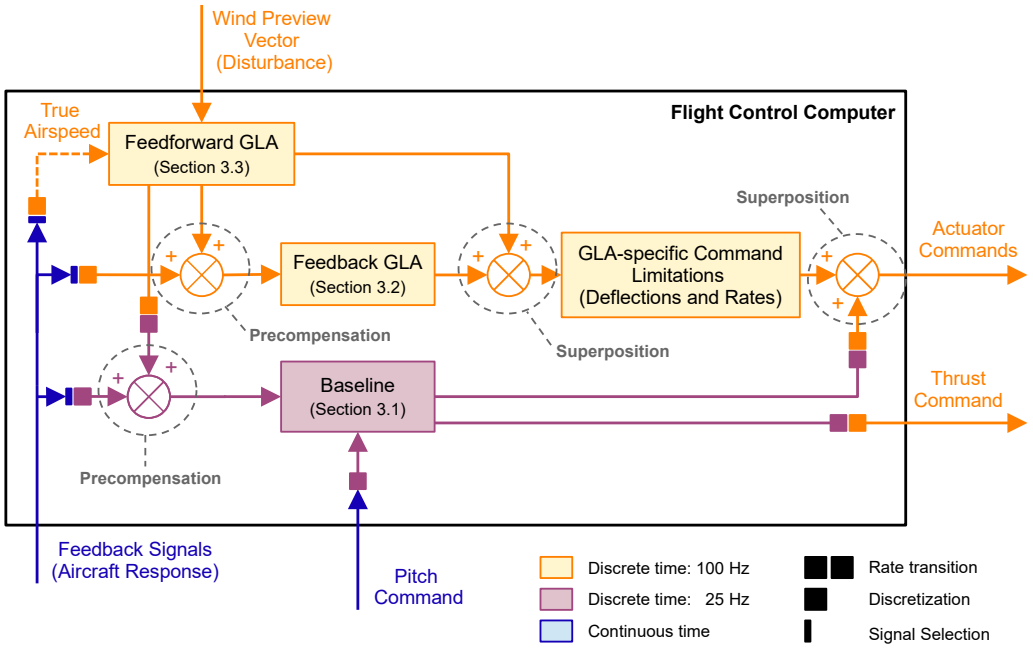

Figure 6: Overview of the 2-DoF Controller Structure (Internal Structure of the Flight Control Computer)

3.1 Baseline Controller

A representative baseline "rigid-body" control function [18–20] is included in the flight control computer (lowermost purple block in Figure 6). The implemented control law was designed manually according to the so-called C*-criteria [21, 22]. It contains both a pilot input feedforward shaping filter and a fairly classical PID-like feedback structure. The feedback part was tuned as a compromise between low feedback gains, robustness to model uncertainties, and disturbance rejection. The pilot input (n_z-based command) feedforward filter is tuned to provide a stick input response according to the C*-upper and -lower limits [21]. The control function commands the aircraft in the pitch axes in the form of controlling the left/right elevator pair. Both surfaces receive the same command, i.e. only symmetrical commands are sent to the actuator model. Such control functions are known to suppress the speed stability. However, the slow drift in speed that could result from it is easy to control. Therefore, the true airspeed is fed back to provide an engine command, varying the thrust (lever) to compensate for the drift in speed. The baseline control function is implemented in a partition of the flight control computer running at 25 Hz (i.e., 40 ms sampling time). Through the sensor measurements (n_z, q, V_{TAS}) used in its feedback path, the function measures the consequences of the encountered gust. It will react to these measurements, and (possibly) interact with the other control functions, which is why it should be considered in the evaluation model. To simplify future references and comparisons, e.g. in future publications, this particular baseline controller is called **DLR-FT-GLRA-BASE-FB-v1** from now on.

3.2 Feedback Gust Load Alleviation Controller Structure Used

The feedback gust load alleviation controller, part of the overall controller structure ("Feedback GLA" in Figure 6), is a single-input-multiple-output (SIMO) state space system running at a discrete sample time of 0.01s (sample rate 100 Hz). To simplify future references and comparisons, e.g. in future publications, this particular feedback controller is called **DLR-FT-GLRA-GLA-FB-v1** from now on. The internal structure is shown in Figure 7. The vertical load factor n_z is the only input of the controller, whereby the outputs of the system consist of

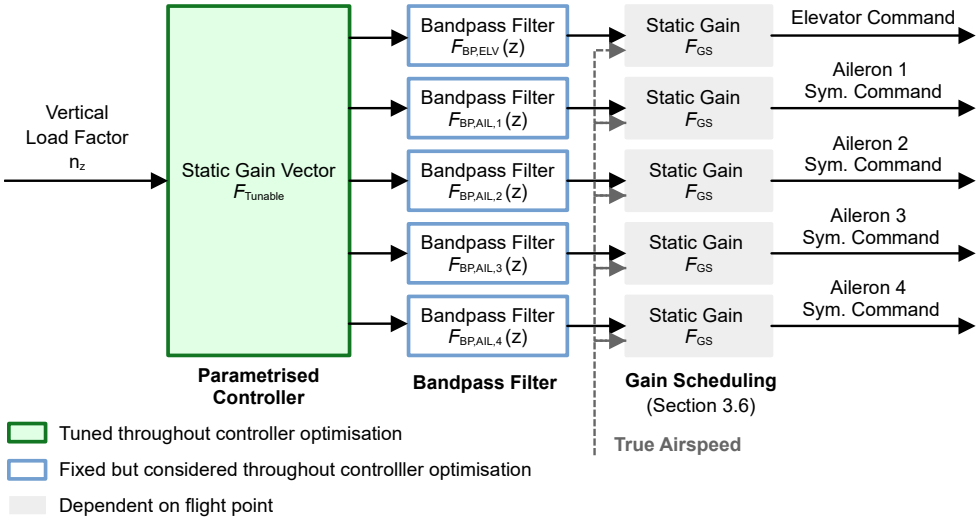

Figure 7: Inner Structure of the Feedback Gust Load Alleviation Control Function

five individual commands for the used control surface pairs (left/right elevators, four pairs of left/right ailerons, from the inner-most position to the outer-most position). Both surfaces of each pair receive the same command, i.e. only symmetrical commands are sent to the actuators. The first part of the controller is parametrised (left green box in Figure 7). This tunable part contains five tunable parameters, composing a static gain vector that provides five individual control surface commands. Each output of this controller part is connected to an individual band-pass filter (boxes outlined in blue in the centre of Figure 7). The filtered individual control surface commands are multiplied afterwards by a static gain factor (rightmost grey boxes in Figure 7), representing the last part of the controller, providing a true airspeed-dependent gain scheduling.

The five individual bandpass filters $F_{\text{BP,ELV}}(z)$, and $F_{\text{BP,AIL,1}}(z)$ to $_{\text{FBP,AIL,4}}(z)$ are defined manually by the designer and are obtained by discretising the following (parametrised) Laplace transfer function (with Tustin's method):

$$F_{\text{BP}}(s) = \overbrace{\frac{s}{(2\cdot\pi\cdot f_{\text{A}})+s}}^{\text{high-pass filter}} \cdot \overbrace{\frac{s}{(2\cdot\pi\cdot f_{\text{B}})+s}}^{\text{high-pass filter}} \cdot \underbrace{\frac{1}{\frac{1}{2\cdot\pi\cdot f_{\text{C}}}\cdot s+1}}_{\text{low-pass filter}} \cdot \underbrace{\frac{1}{\frac{1}{2\cdot\pi\cdot f_{\text{D}}}\cdot s+1}}_{\text{low-pass filter}}. \tag{1}$$

Each symmetrical control surface command is filtered by an individual bandpass filter, which consists of different cut-off frequencies for the low-pass part as well as for the high-pass part. The chosen frequencies are shown in the Table 3.

Table 3: Cut-Off Frequencies of the Bandpass Filters for the Feedback Gust Load Alleviation Controller

	f_{A} [Hz]	f_{B} [Hz]	f_{C} [Hz]	f_{D} [Hz]
$F_{\text{BP,ELV}}(s)$	2.0	2.0	4.0	9.0
$F_{\text{BP,AIL,1}}(s)$	0.1	0.1	9.0	9.0
$F_{\text{BP,AIL,2}}(s)$	0.1	0.1	9.3	9.3
$F_{\text{BP,AIL,3}}(s)$	0.1	0.1	7.7	7.7
$F_{\text{BP,AIL,4}}(s)$	0.1	0.1	10.3	10.3

These filters are part of the controller structure during tuning. The tunable part of the controller can, therefore, account for them, even if it is not allowed to tune them. Cutting the lowest

frequencies ensures that no constant or quasi-constant deflections can be commanded, which is desirable. In the pitch axis, such constant deflection would interact with the aircraft trim and the flight mechanics. On the ailerons, this would impact the flight shape of the wing and the flight performance. Cutting the highest frequencies limits the sensitivity of the control function to higher-modes and uncertainties, and prevents propagating noise of the measured vertical load factor n_z to the control surfaces.[3]

3.3 Feedforward Gust Load Alleviation Controller Structure Used

In contrast to the feedback GLA controller, the feedforward GLA controller consists not only of the control function, but also of a so-called prediction model (Figure 8). The feedforward GLA function is presented in Subsection 3.3.1, the precompensation mechanism including the prediction model in Subsection 3.3.2.

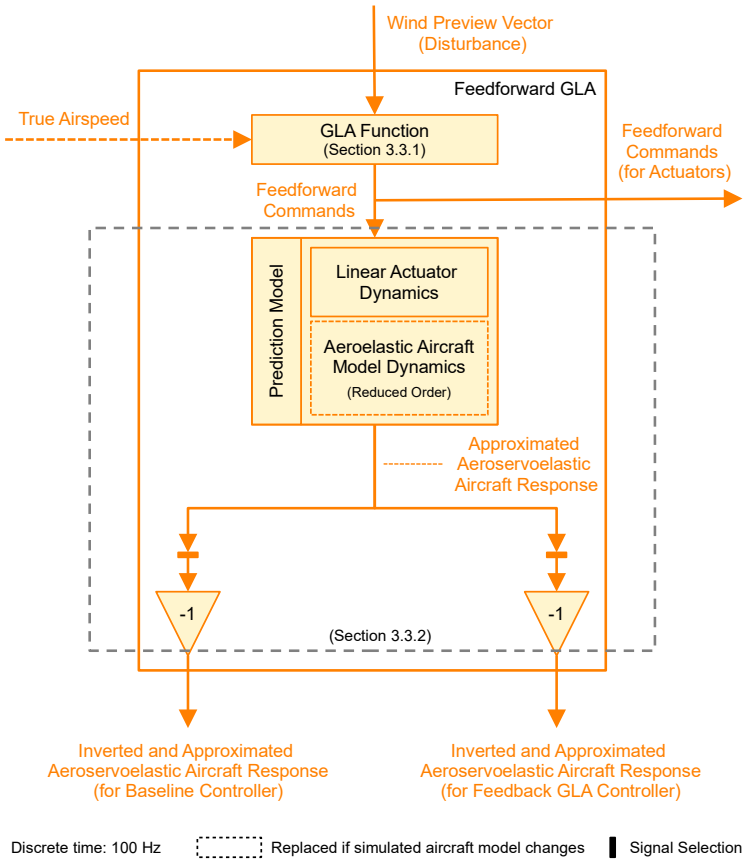

Figure 8: Detailed View into the Structure of the Feedforward GLA Controller

3.3.1 GLA Function

The control function is (non-considering the nonlinear SSBS-filter element, see below) a multiple-input-multiple-output (MIMO) state space system running at a discrete sample time of 0.01 s (sample rate 100 Hz). To simplify future references and comparisons, e.g. in future publications, this particular feedforward control function is called **DLR-FT-GLRA-GLA-FF-v2** from now on. The implemented control law is a redesigned version of the feedforward control function (DLR-FT-GLRA-GLA-FF-v1) presented in [12]. The control function consists of

[3]It should be noted at this point that feedback noise, in general, is not part of the executed simulations. In real applications, a certain amount of noise is to be expected and the omission of a low-pass-output filter would probably lead to a too optimistic load alleviation performance.

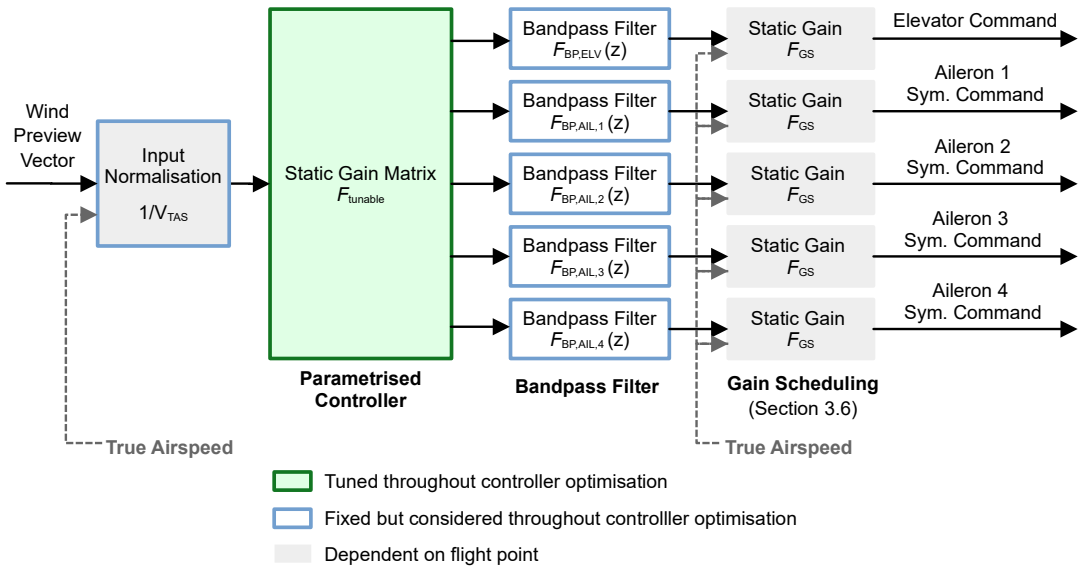

Figure 9: Inner Structure of the Feedforward Gust Load Alleviation Control Function

a parametrised (i.e. tunable), a fixed (bandpass filter), and a gain-scheduled part connected in series (the inner structure of the control function is shown in Figure 9). The input of the control function consists of the wind preview vector (Subsection 2.2). The outputs of the control function consist of five individual commands for the used control surface pairs (left/right elevators, four pairs of left/right ailerons, from the inner-most position to the outer-most position). Both surfaces of each pair receive the same command, i.e. only symmetrical commands are sent to the actuators. Identical actuator commands are also forwarded to the second sub-part of the controller structure, the prediction model (Figure 8). This prediction model is implemented for the purpose of precompensation (Figure 6), which is described in detail in Section 3.3.2.

As a part of the feedforward controller structure, the estimated vertical wind vector is additionally filtered by a so-called "smooth sigmoid-based shrinkage" (SSBS) function[4] [11, 23] (not illustrated in Figure 9). Such a nonlinear function enables to set the amplitudes of wind speeds below a predefined threshold value to zero. Small and therefore uncritical vertical winds can be caused either by negligible atmospheric disturbances or artificially by the influence of measurement inaccuracies and noise. Not taking noise-like information into account suppresses unnecessary control surface activities and extends the service life of the actuating system. At the same time, wind speeds above a certain threshold value are fully taken into account. The transition between the two conditions can be made smooth. Logically, such a nonlinear element cannot be part of the standard linear control synthesis problem, which is why it is subsequently integrated into the controller structure and not taken into account during tuning. For easier interpretation, the previewed vector is afterwards normalised by dividing the vertical wind velocities with the true airspeed.

The first part of the control function is parametrised (left green box in Figure 9), receiving the entire preview vector with 83 elements described above. This tunable part is composed of a 5×83 static gain matrix, providing five individual control surface commands. This leads to a total of 415 tunable parameters. Even if the parametrised part of the controller is here defined as a static gain matrix, the transfer function from the vertical wind/gust to the output of the control function should be seen as a finite impulse response (FIR) filter: the previewed wind vector can be seen as a tapped delay line and the gain matrix as the FIR filter gains ([7, 24]).

[4]The used parameters for the SSBS-function are: $t = 0.0$, $\lambda = 3.2$, $\tau = 4.0$.

The tuning and the number of preview and postview elements were defined based on the most critical flight point, the flight point with the highest true airspeed in this case. For lower speeds, it could make sense to increase the number of preview and postview elements. As shown above, the number of preview elements is defined based on an effective measurement range and the number of time steps needed to cover this distance. At lower speeds, it would potentially take more time steps to cover the same distance and hence h_{preview} (Subsection 2.2) could be increased. Similarly, the number of time steps needed for the tail of the aircraft to reach the current position of the chosen reference position also becomes larger. For simplicity, the number of preview and postview elements were kept constant, which means that they are slightly suboptimal for lower speeds.

Each output of this control function is connected to an individual bandpass filter (boxes outlined in blue in the centre of Figure 9). The five individual bandpass filters $F_{\text{BP,ELV}}(z)$, and $F_{\text{BP,AIL,1}}(z)$ to $_{\text{FBP,AIL,4}}(z)$ are defined manually by the designer and are obtained by discretising the following (parametrised) Laplace transfer function (with Tustin's method):

$$F_{\text{BP}}(s) = \overbrace{\frac{s}{(2 \cdot \pi \cdot f_{\text{A}}) + s}}^{\text{high-pass filter}} \cdot \underbrace{\frac{1}{\frac{1}{2 \cdot \pi \cdot f_{\text{B}}} \cdot s + 1}}_{\text{low-pass filter}} \cdot \underbrace{\frac{1}{\frac{1}{2 \cdot \pi \cdot f_{\text{C}}} \cdot s + 1}}_{\text{low-pass filter}}. \tag{2}$$

Each symmetrical control surface command is filtered by an individual bandpass filter, which consists of different cut-off frequencies (frequencies are shown in Table 4) for the low-pass part as well as for the high-pass part. Concerning the cut-off frequencies, the same design criteria and assumptions as in Section 3.2 were used to design the implemented filters.

Table 4: Cut-Off Frequencies of the Bandpass Filters for the Feedforward Gust Load Alleviation Control Function

	f_{A} [Hz]	f_{B} [Hz]	f_{C} [Hz]
$F_{\text{BP,ELV}}(s)$	0.2	3.0	5.0
$F_{\text{BP,AIL,1}}(s)$	0.2	4.0	7.0
$F_{\text{BP,AIL,2}}(s)$	0.2	6.0	7.0
$F_{\text{BP,AIL,3}}(s)$	0.2	5.0	7.0
$F_{\text{BP,AIL,4}}(s)$	0.2	9.0	9.0

3.3.2 Interconnecting Feedforward and Feedback Control Laws

The feedforward control law is providing its commands both to the actuators of the aircraft, and to the prediction model. The purpose of the prediction model is to provide an approximated response of the full-order aeroservoelastic aircraft model, based only on the feedforward GLA commands. The feedforward GLA commands lead to an intended reaction of the aircraft, even before the aircraft nose encounters the gust. The trajectory of the aircraft is changed via elevator commands in the pitch axes to partly compensate for the expected change in angle of attack (due to the upcoming gust), and via aileron commands which are used to shift the wing lift in lateral direction. The initiated manoeuvre corresponds to varying values in feedback channels used by the feedback controller. The feedback controller functions presented in Subsection 3.1 and 3.2 cannot distinguish whether the reason of varying values of the feedback channels they use is induced by a disturbance, or by feedforward controller commands. Regardless of the cause, all feedback control functions will potentially react to the varying feedback signals in terms of their implemented control laws, leading to a (partly) compensation of the feedforward controller

commands, which results in a significantly worse load alleviation performance. Calculated with the prediction model, the incremental and approximated aircraft response is inverted (Figure 8) for the purpose of precompensation, and superimposed on the feedback signals (Figure 6).

The prediction model consists of two components, linear actuator dynamics and a significantly reduced linear aeroelastic aircraft model. The actuators are represented by a state-space system of 10^{th} order (denoted by low-pass filter characteristics of second order for each actuator), the linear part of the nonlinear actuator dynamics shown in Table 2. The aeroelastic aircraft part is represented by a linear state-space system, which is reduced to a system of 20^{th} order, a size below 1 % of its original size. Based on the available aircraft models (Table 1), 54 prediction models are disposable. The implemented actuator dynamics are fixed, but the prediction model is continuously adapted to the simulated aircraft model.

3.4 Creating Specific Aircraft Models for the GLA Controller Synthesis/Tuning

Integrated aeroelastic aircraft models composed by the modelling approach VarLoads are well suited for the simulation of modern, flexible aircraft during flight through atmospheric disturbances. However, they bear a certain complexity with typically a few thousand states and quite high-frequency modes. These models are too complex for the robust control methods used to obtain both the feedforward gust load alleviation function as well as the feedback gust load alleviation function. In this word, the algorithms from the MATLAB® Control System and Robust Control toolboxes are used. These tools have drastically improved over the last twenty years, yet still a significant reduction of the models used is required.

In such reduction, a certain trade-off between size and representativeness of the models needs to be made. Further modifications/transformations are also needed to obtain a model that can be used for discrete-time H_∞ or H_2 control synthesis. The original aeroelastic models are built with different zones with separate wind inputs for each zone and with separate inputs for wind/control surface deflections and their time-derivatives. They are transformed using Padé approximations [25] to account for time delays. Pseudo-differentiator filters (e.g. $s/(\epsilon\, s + 1)$ with a small value for ϵ compared to the inverse of the frequencies that need to be controlled) are used to replace groups of inputs which are time-derivatives of each other with a single equivalent input. After several iterations on the model reduction parameters (scaling, order, etc.), the models were reduced from almost 3000 thousands to about 100 states. Discrete-time models are generated by discretising the reduced continuous-time models. In the case of the feedforward control function, the discrete models are augmented by a linear filter representing realistic lidar and wind reconstruction capabilities [7]. Finally, some of its transfers are normalised, eventually weighted and/or augmented with linear actuator dynamics to obtain a standard control synthesis problem [8,9,12] on which the synthesis is made in discrete time. In the feedback case, the lidar representation is not needed and therefore not included in the design model.

To save time during the design of the gust load alleviation controllers, intermediate evaluations are performed using simplified models (compare to the hybrid simulation shown in Figure 3. The quickest and simplest validation option directly uses the designed controller with the (discrete) model it has been designed for. Evaluating the controllers with the design models or some other reduced models is useful as the actual targets in terms of gust load alleviation, e.g. peak load in response to a one-minus-cosine gust, are not easy to formulate with frequency-domain criteria [26]. When the load alleviation performance of the tuned control function is deemed satisfactory on these models, then it is worth performing a more precise evaluation of its performance using the heavier and more time-consuming multi-rate hybrid simulation envi-

ronment. All results shown in this paper were computed using the multi-rate hybrid simulation from Figure 3.

3.5 Multi-Model Iterative Tuning of the Gust Load Alleviation Control Functions

The tuning of gust load alleviation functions is almost never done in a single pass, but rather an iterative process in which the control synthesis is only a step. There are two main reasons for this. First, it is not always possible to define the correct values for all weighing functions or templates beforehand. Whilst the reduction of the gust response to a certain level can be fairly well specified on its own, the trade-off between different load types and stations across the airframe, in combination with the control surface activity, often requires the designer to weigh different options, analyse them in simulation (potentially with various levels of representativeness of the simulation environment used), and loop back with slightly adjusted specifications. For conciseness reasons, this iterative process is not detailed further, but the interested reader can refer to the process shown in [8, Figure 1], as it corresponds to the process also used in the present work.

Tuning of the Feedback Gust Load Alleviation Function

Table 5: H_∞-Optimisation Criteria for the Feedback GLA Control Function

No.	Input	Output	Template in Frequency Domain	f, Hz
1	α_{gust}	WRBM	0.92	[0.025, 10]
2	α_{gust}	$\dot{\eta}_{sym}$	60.00	[0.025, 10]
3	α_{gust}	$\dot{\xi}_{ail,sym,1}$	38.00	[0.025, 10]
4	α_{gust}	$\dot{\xi}_{ail,sym,2}$	38.00	[0.025, 10]
5	α_{gust}	$\dot{\xi}_{ail,sym,3}$	38.00	[0.025, 10]
6	α_{gust}	$\dot{\xi}_{ail,sym,4}$	38.00	[0.025, 10]

Based on the analysis of the open-loop gust load behaviour of the aircraft (Figure 5), eight different aircraft models were finally selected for the tuning of the feedback gust load alleviation function. They correspond to the mass cases with the highest total mass (MZmMe, MTFFJ, MTAAJ, MTmMG) at the flight point at the highest true airspeed / highest altitude (equivalent to Flight Point 3 in Figure 5), including both the "clean-wing" and the "airbrake-out" wing configuration.

In case of the feedback GLA function a template was defined to optimise the frequency response behaviour between the wind input and the bending moment output at the wing root (first optimisation criteria in Table 5). Whilst reducing the wing root bending moment (WRBM) was top priority, excessively large and fast control surface commands should be prevented. For this, further criteria were added during the tuning. The limits on the control surface deflections were defined in such a way (second to fifth criterion in Table 5) that the specifications regarding control surface rates (Table 2) are not to be expected to be exceeded in the subsequent evaluations with the certification gusts.

The final multi-model tuning (the associated standard control synthesis structure is shown e.g. in [27]) of the feedback GLA function was performed with the eight aircraft models selected, each combined with the six different criteria (Table 5), so 48 performance channels in total. A good trade-off between the different control objectives was rapidly obtained. The controller made good use of the available authority on the ailerons and elevators to obtain a very significant loads reduction, while not being exaggeratedly aggressive.

Tuning of the Feedforward Gust Load Alleviation Function

Table 6: H_∞-Optimisation Criteria for the Feedforward GLA Control Function

No.	Input	Output	Template in Frequency Domain	f, Hz
1	α_{gust}	WRBM	$T_{\text{WRBM}}(s)$	[0.025, 10]
2	α_{gust}	$\dot{\eta}_{sym}$	$T_{\text{ELV}}(s)$	[0.025, 10]
3	α_{gust}	$\dot{\xi}_{ail,sym,1}$	$T_{\text{AIL}}(s)$	[0.025, 10]
4	α_{gust}	$\dot{\xi}_{ail,sym,2}$	$T_{\text{AIL}}(s)$	[0.025, 10]
5	α_{gust}	$\dot{\xi}_{ail,sym,3}$	$T_{\text{AIL}}(s)$	[0.025, 10]
6	α_{gust}	$\dot{\xi}_{ail,sym,4}$	$T_{\text{AIL}}(s)$	[0.025, 10]

The tuning of the feedforward control law has substantial similarity to the tuning of the feedback gust load alleviation control function. Naturally, compared to the design models used for the feedback GLA, the aeroservoelastic design models here were additionally augmented with lidar capabilities, providing 83 approximated wind measurements channels. As presented in [12] and compared to the work shown in [8], the iterative process was made easier by combining it with the linear filter approximation of the lidar-based wind estimation losses proposed in [7]. Due to similar optimising criteria concerning the load distribution and the control surface activities, the final choice of the performance channel is comparable with the feedback GLA tuning. In contrast to the constant templates presented in Table 5, the feedforward GLA control law was tuned with more complex templates (Table 6), a bandpass filter

$$T_{\text{WRBM}}(s) = 0.925 \cdot \overbrace{\frac{s}{(2\cdot\pi\cdot 0.3)+s}}^{\text{high-pass filter}} \cdot \overbrace{\frac{s}{(2\cdot\pi\cdot 0.7)+s}}^{\text{high-pass filter}} \cdot \underbrace{\frac{1}{\frac{1}{2\cdot\pi\cdot 2.5}\cdot s+1}}_{\text{low-pass filter}} \cdot \underbrace{\frac{1}{\frac{1}{2\cdot\pi\cdot 7.5}\cdot s+1}}_{\text{low-pass filter}}, \tag{3}$$

was used for first performance channel and band-stop filters were used for the elevator and aileron deflection rates, repectively:

$$T_{\text{ELV}}(s) = 24.50 \cdot \underbrace{\frac{1}{\frac{1}{2\cdot\pi\cdot 1.525}\cdot s+1}}_{\text{low-pass filter}} \cdot \overbrace{\frac{s}{(2\cdot\pi\cdot 2.200)+s}}^{\text{high-pass filter}}, \tag{4}$$

$$T_{\text{AIL}}(s) = 35.00 \cdot \underbrace{\frac{1}{\frac{1}{2\cdot\pi\cdot 1.515}\cdot s+1}}_{\text{low-pass filter}} \cdot \overbrace{\frac{s}{(2\cdot\pi\cdot 2.215)+s}}^{\text{high-pass filter}}. \tag{5}$$

The band-stop filter were used to penalise a too aggressive behaviour of the control surfaces due to a specific range of non-critical gust cases (around a gust length of 67 m, according to [24] equivalent to a characteristic gust frequency of 1.972 Hz) at the critical and therefore tuning flight point.

3.6 Gain Scheduling of the Gust Load Alleviation Functions

Both gust load alleviation control laws were tuned using aircraft models corresponding only to the fastest flight point. To adapt the control laws to less critical flight points, a gain-scheduling strategy was identified and applied to the static gain part F_{GS} of the feedback GLA controller

(Figure 7) and the feedforward GLA controller (Figure 9). The strategy build on the true airspeed (the available flight points are denoted by a constant equivalent airspeed), according to the following equation

$$F_{\mathrm{GS}}\left(\mathrm{V}_{\mathrm{TAS}}\right) = \left(\frac{V_{\mathrm{TAS}}}{V_{\mathrm{TAS,ref}}}\right)^2 = \left(\frac{V_{\mathrm{TAS}}}{V_{\mathrm{TAS,FP,3}}}\right)^2, \tag{6}$$

aiming to modify the controller gains for lower speeds. The true airspeed of the most critical flight point is taken as the reference speed. In case of the feedforward GLA function, the gain scheduling also includes the input normalisation (Figure 9). Hence, unlike in the case of the gain scheduling of the feedback GLA, a choice of at least > 1 for the exponent in Equation (6) leads to reduced gains for the non-critical flight points, in which an increasing order of the exponent leads to decreasing gains.

4 ACTIVE LOAD CONTROL RESULTS

In this Section, the impacts of the particular controller functions on the aircraft behaviour are discussed. Subsection 4.1 discusses the influence of the individual controller functions on the structural load behaviour of the wing quantitatively. The results relate to the distribution of the bending moment and the torsional moment for the wing structure, each broken down by flight points. Subsection 4.2 illustrates the time behaviour of the entire 2-DoF controller structure using an exemplary (and critical) gust load case. The behaviour without and with activated precompensation is considered. Finally, Subsection 4.3 summarises the quantitative load alleviation performance achieved by the 2-DoF controller structure, clearly showing the influence of precompensation.

4.1 Quantitative Load Alleviation Analysis of Particular Controller Functions

Even if not intended, the baseline controller function impacts the overall load hierarchy (Figure 10). Due to the commands in the pitch axis, the structural bending loads on the inner wing are reduced slightly. However, the peak bending moments on the outer wing are marginally deteriorated. In contrast, the resulting torsional moments on the inner wing, between the engine pylon and the wing root, are considerably worse. This is probably caused by varying engine thrust forces, trying to compensate for speed shifts during the gust encounter. A reversal of the flight point-dependent the load hierarchy does not occur, neither for the bending moment nor the torsional moment.

The tuned feedback GLA controller function offers, under consideration of the gain scheduling strategy, a satisfactory performance in terms of alleviating the bending loads both at the wing root and over the entire wing span (Figure 10). The achieved bending moment load alleviation performance varies between around 0 % near the wing tip, about 4 % at the wing root and up to approximately 8 % close to the ailerons. The peak torsional moment distribution is, on the one hand, slightly deteriorated for the area between the engine pylon and the ailerons, respectively, the wing root. On the other hand, the torsional load envelope could have been improved along the rest of the wingspan (neglecting the outermost load station). Similar to the load envelopes for the baseline controller, a reversal of the load hierarchy could be prevented.

The implementation of a gain scheduling strategy according to Equation (6) offers a satisfactory performance for the feedforward GLA function in terms of alleviating the bending loads both at the wing root and over the entire wingspan (Figure 10). The feedforward GLA controller achieves a bending moment load alleviation performance at the wing root between 17 % and

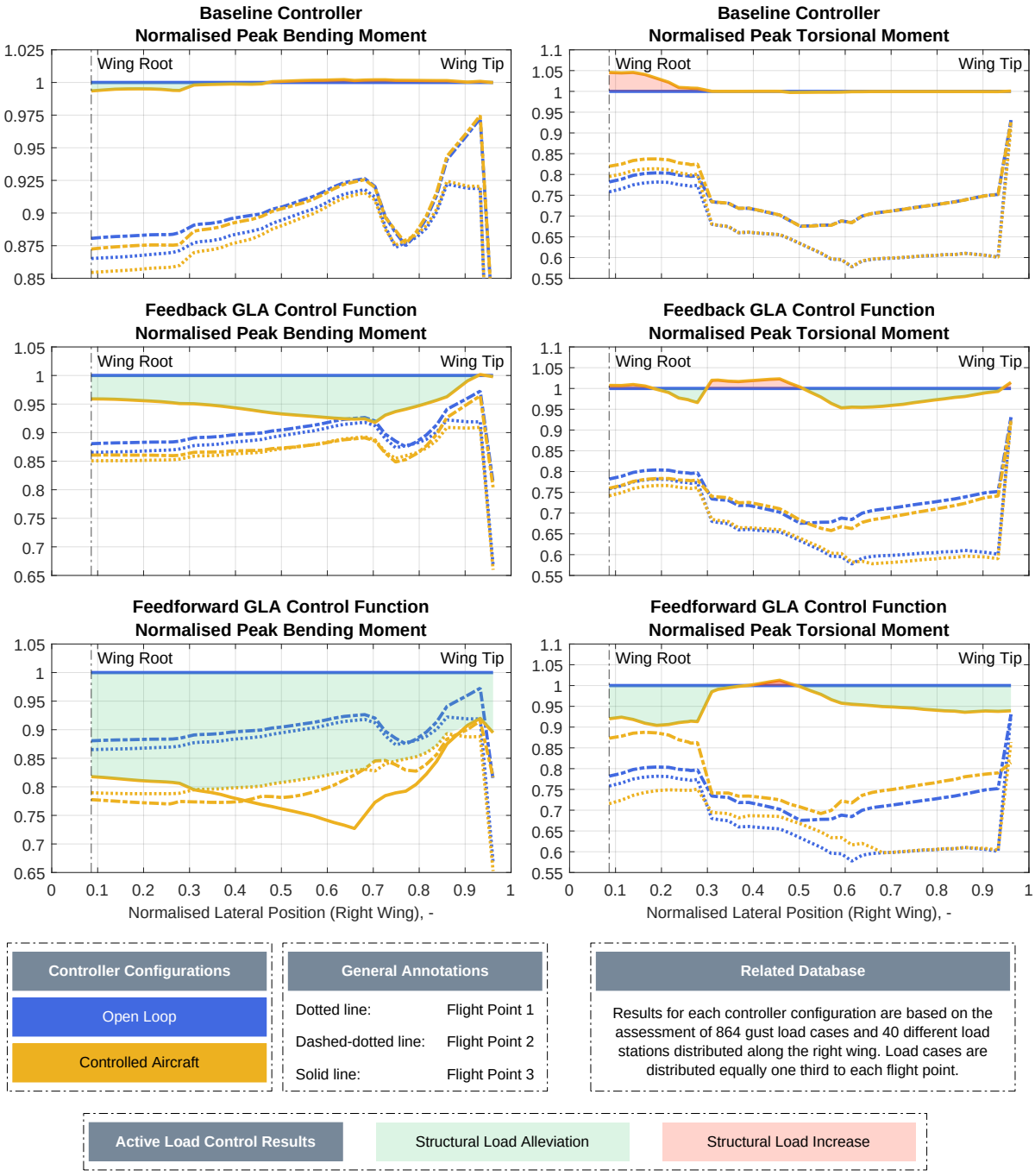

Figure 10: Distribution of Structural Loads shown for the Aircraft Wing, evaluated without Control and with each Control Function separately, broken down by Flight Points

18%, and the load reduction increases up to around 20 % at mid-wing. A reversal of the load hierarchy could not be prevented. The bending loads of the controlled aircraft for flight points 1 and 2 at the important wing root are below those of flight point 3. At the same time, for the centre of the wing the alleviated loads of flight point 1 and flight point 2 are greater than the loads at flight point 3. If the bending loads at flight point 3 in this area were still dominant, the load alleviation performance achieved could be increased even further. The application of the feedforward GLA controller improves the torsional moment almost along the entire wingspan. It is slightly increased only in an area between the engine pylon and the ailerons. Similar to the bending moment distribution, the load hierarchy of the torsional moment has also changed. However, this has no influence on the overall performance.

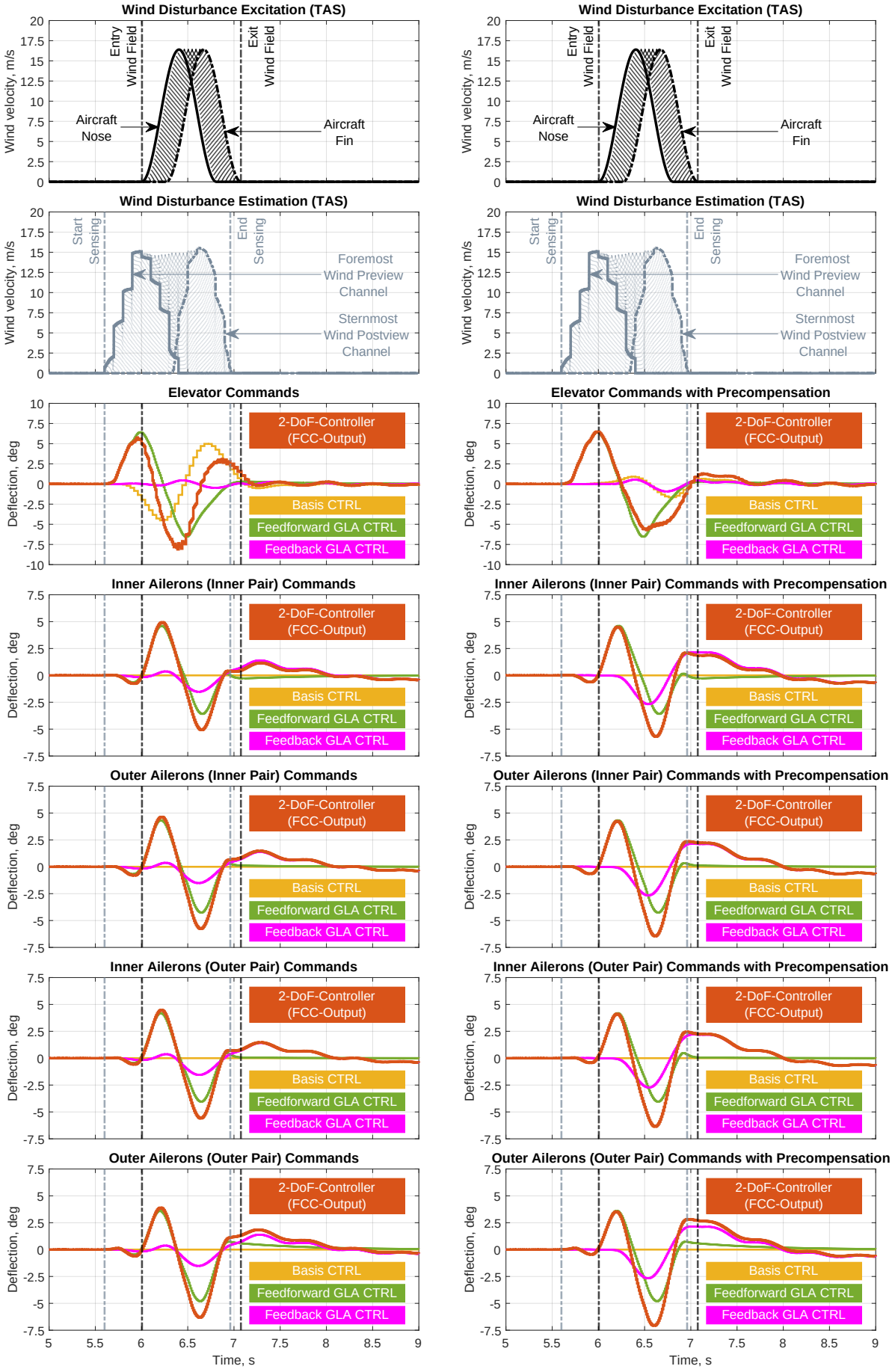

Figure 11: Exemplary Aircraft Excitation Results in Time Domain for Mass Distribution MTmMG, Speed V_C and Altitude 8300 m in "Clean"-Wing Configuration for Upward Gust with Gust Length of 107 m

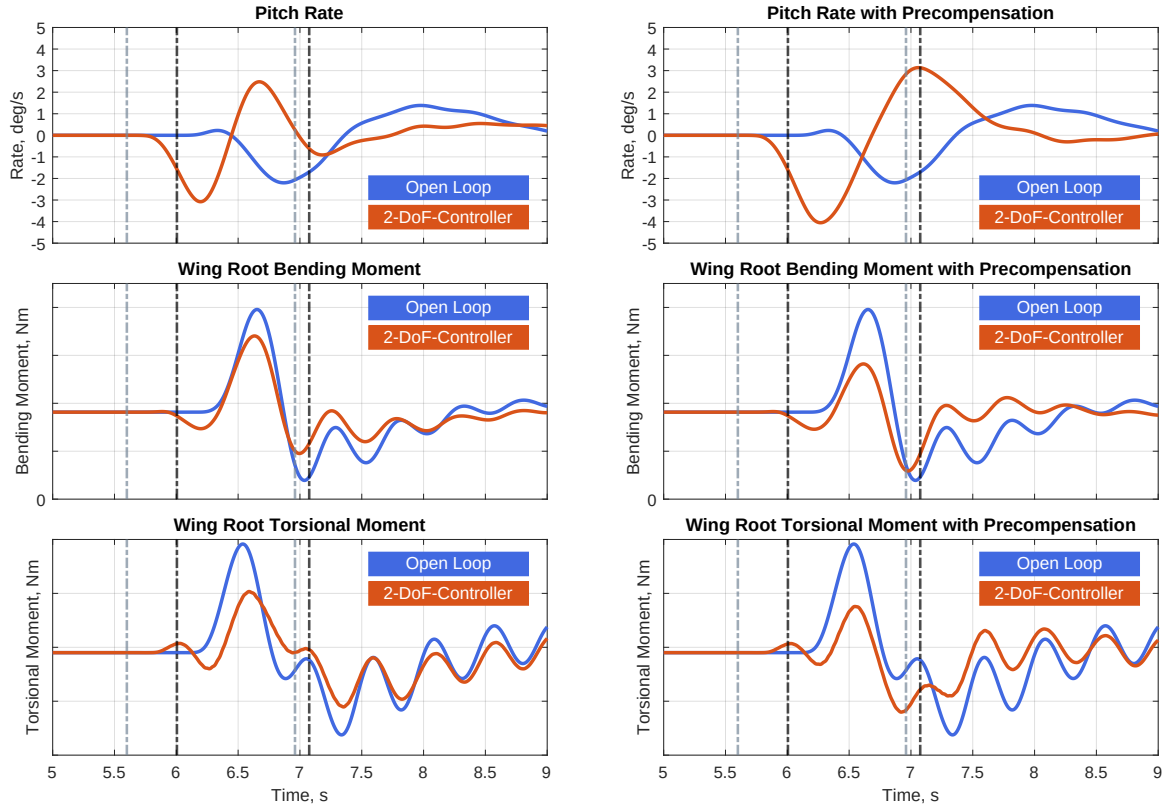

Figure 12: Exemplary Aircraft Response Results in Time Domain for Mass Distribution MTmMG, Speed V_C and Altitude 8300 m in "Clean"-Wing Configuration for Upward Gust with Gust Length of 107 m

4.2 Qualitative Analysis of the Time Behaviour of the 2-DoF-Controller

Exemplary results in time domain for a sizing gust load case with precompensation (plots in right column) and without precompensation (plots in left column) are illustrated in Figure 11 and Figure 12. The complete 2-DoF-controller structure is active, all control functions providing individual commands for the control surfaces. The top two rows in Figure 11 show the excitation of the aircraft by the wind field and the corresponding wind estimates, which are forwarded to the feedforward GLA function as the preview vector. The passage of the gust from the nose to the end of the aeroplane determines the time range of the external wind excitation. The wind preview vector determines the time range of the wind field sensing, which starts before the gust encounter. As can be seen for all control surface command plots, the commands of the feedforward GLA function starting slightly after the beginning of the gust sensing. The four independent aileron commands (2-DoF-Controller / FCC Output) consists of commands from the feedforward GLA function and the feedback GLA function. Without precompensation, each symmetric aileron command of the feedback GLA function starts between the gust sensing and the wind disturbance excitation, as a reaction to the manoeuvre initialised by the feedforward GLA function. With precompensation, each symmetric aileron command is starting after the beginning of the wind disturbance excitation, as a reaction to the gust and not the manoeuvre initialised by the feedforward GLA function. The advantages of the precompensation become even clearer when looking at the elevator commands. The superposed elevator command (2-DoF-Controller / FCC Output) consists of commands provided by the baseline controller and both GLA functions. Without precompensation, especially the baseline controller starts to provide a deflection slightly after the beginning of the wind disturbance sensing, but before the gust encounter. The baseline command for the elevator deflection is, compared to the feedforward GLA command, of opposite direction, derogating the full superposed elevator command (2-DoF-Controller / FCC Output). If the precompensation is activated, the elevator command

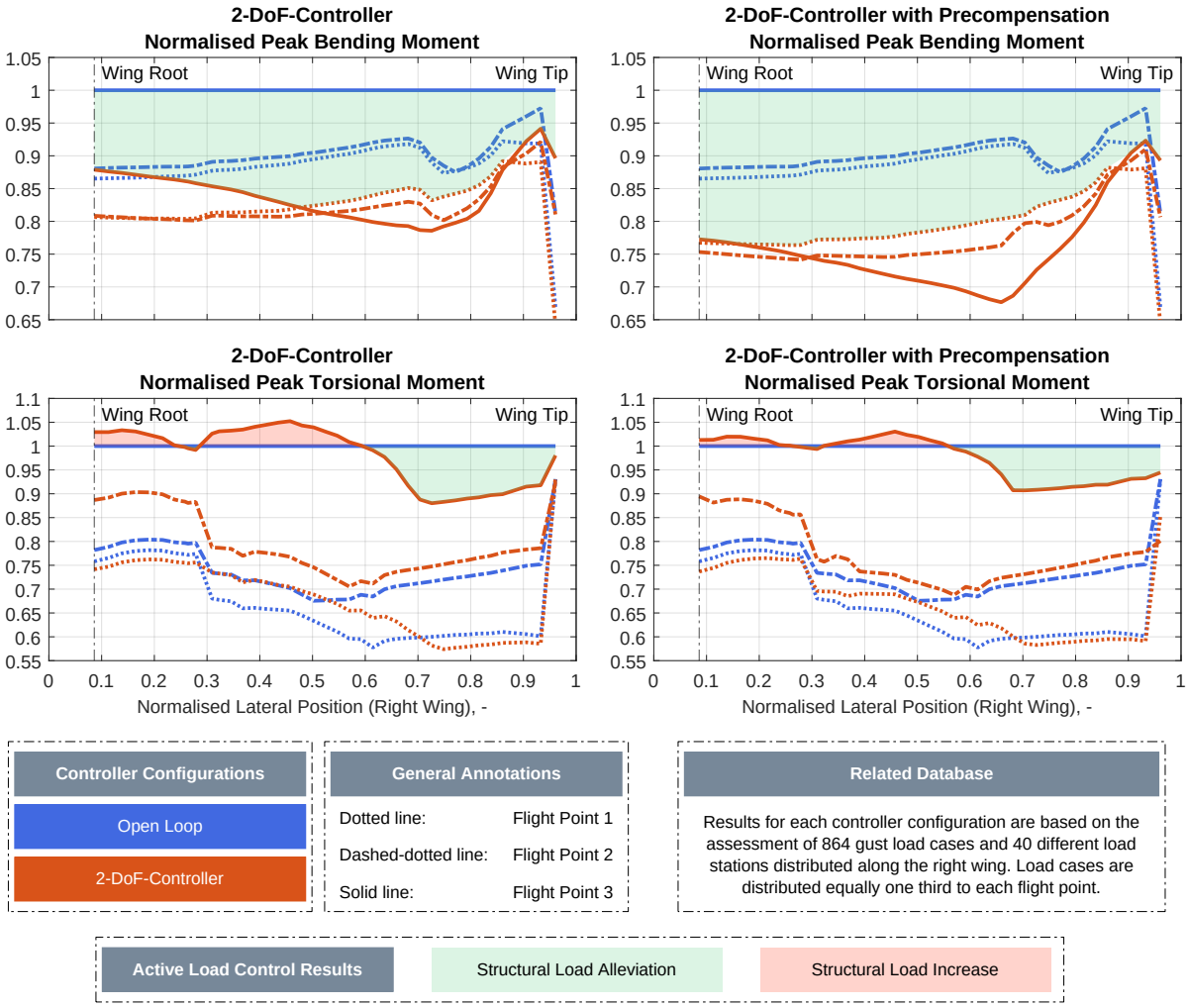

Figure 13: Distribution of Structural Loads shown for the Aircraft Wing, without Control and with the 2-Degree-of-Freedom Controller (Left Side simulated without Precompensation / Right Side simulated with Precompensation), broken down by Flight Points

of the baseline controller is (nearly) completely leveled out until the aircraft response due to the gust is measured. The derogation of the superposed elevator command (2-DoF-Controller / FCC Output) is (nearly) fully suppressed.

As can be seen in Figure 12, the achieved pitch rate, initialised by the feedforward GLA control function, is significantly larger if the precompensation is activated. The precompensation also has a distinctive influence on the loads, as can be seen especially for the bending moment loads at the wing root. The achieved level of load alleviation is significantly larger than without precompensation.

4.3 Quantitative Analysis of the 2-DoF-Controller

The load alleviation results for the 2-DoF-controller structure (all control functions are active) are illustrated in Figure 13. Both the bending moment distribution and the torsional moment distribution are presented for the wing. The left column shows the results simulated without precompensation, the right column presents the results simulated with an activated precompensation. The precompensation has a significantly influence on the loads, especially for the load distribution of the most critical flight point 3. Without precompensation, the achieved bending moment load alleviation at the wing root reaches a level of about 11 % to 12 %, compared to the open loop case. This performance derogation is caused by insufficiently alleviated peak

loads at flight point 3. Due to the finally chosen scheduling strategy, the (in terms of structural loads) most critical flight point is denoted by the most aggressive GLA-controller commands. A non-activated precompensation therefore has a particularly counterproductive effect at this flight point. The achieved level of load alleviation is worse than the performance achieved with the feedforward GLA controller alone (Figure 10). With an activated precompensation, the achieved level of load reduction for the bending moments for the closed-loop configuration are significantly higher than without precompensation. At the important wing root, about 22 % to 23 % load reduction is achieved and the bending load alleviating potentials of all three control functions are nearly superposed. Furthermore, the raise in torsional moment distribution along the wingspan turns out much less than without precompensation.

5 SUMMARY AND OUTLOOK

The design of a lidar-based 2-DoF controller structure for load alleviation purposes for a long range aircraft configuration was presented. The gust load alleviation part of the controller structure was scheduled with the true airspeed to account for the change in behaviour of the dynamic model as well as the fact that all flight points are not equally critical in terms of structural gust loads. The complete control architecture was evaluated using a multi-rate hybrid simulation environment with the load alleviation controllers in discrete time and considering a detailed lidar sensor model and the related post-processing algorithms. The 2-DoF controller structure includes a precompensation that is derived from a reduced order model. It prevents the feedback controller from seeing the actions of the feedforward controller as perturbations which needs to be corrected. This proposed compensation was shown to be very effective and the combination of all controllers achieves a quite significant reduction of the peak bending moments along the wing: about 22–23 % around wing root, over 20 % load alleviation from the wing root to about two third of the wingspan, and then reducing to about 10 % improvement near the wing tip. Despite the inclusion of a baseline controller, which is associated with an increased torsional moment, the increase in the torsional moment is kept within a few percents. In the outer wing area, the torsional moment could even be reduced by up to almost 10 %. Further investigations are necessary to robustify the two-degree-of-freedom controller structure. Presently, the prediction model used for the precompensation is adjusted for the different loading cases, which would probably be difficult to implement in practice as the exact loading of the aircraft is often quite uncertain. Nevertheless, the precompensation made is mostly useful for rather low frequencies and it should be possible to use more generic models, with no or less scheduling, without losing too much performance.

ACKNOWLEDGMENTS

This work was performed and funded within the framework of the German national research project InFlyTec (Förderkennzeichen 20A1705C) and within the framework of the German national research project INTELWI (Förderkennzeichen 20A1903A). The authors thankfully acknowledge the funding received from the Federal Ministry for Economic Affairs and Climate Action (BMWK).

6 REFERENCES

[1] Fezans, N. and Joos, H.-D. (2016). Combined lidar-based feedforward and feedback gust and turbulence load alleviation. In *Greener Aviation 2016 Conference*. Brussel, Belgium.

[2] Jenaro Rabadan, G., Schmitt, N. P., Pistner, T., et al. (2010). Airborne lidar for automatic feedforward control of turbulent in-flight phenomena. *Journal of Aircraft*, 47(2), 392–403. doi: 10.2514/1.44950.

[3] Fezans, N., Joos, H.-D., and Deiler, C. (2019). Gust load alleviation for a long-range aircraft with and without anticipation. *CEAS Aeronautical Journal*, 10, 1033–1057. doi: 10.1007/s13272-019-00362-9.

[4] Fezans, N., Vrancken, P., Linsmayer, P., et al. (2020). Designing and maturating doppler lidar sensors for gust load alleviation: Progress made since AWIATOR. In *Proceedings of the Aerospace Europe Conference*. Bordeaux, France: CEAS / 3AF.

[5] Kiehn, D., Fezans, N., Vrancken, P., et al. (2022). Parameter analysis of a doppler lidar sensor for gust detection and load alleviation. In *IFASD 2022*. Madrid, Spain. IFASD-2022-105.

[6] Fezans, N., Schwithal, J., and Fischenberg, D. (2017). In-flight remote sensing and identification of gust, turbulence, and wake vortices using a Doppler LIDAR. *CEAS Aeronautical Journal*, 8(2), 313–333. doi: 10.1007/s13272-017-0240-9.

[7] Cavaliere, D., Fezans, N., and Kiehn, D. (2022). Method to account for estimator-induced previewed information losses - application to synthesis of lidar-based gust load alleviation functions. In *CEAS EuroGNC 2022*. Berlin, Germany.

[8] Fezans, N., Wallace, C., Kiehn, D., et al. (2022). Lidar-based gust load alleviation - results obtained on the Clean Sky 2 Load Alleviation Benchmark. In *IFASD 2022*. Madrid, Spain. IFASD-2022-155.

[9] Wallace, C., Schulz, S., Fezans, N., et al. (2022). Evaluation environment for cascaded and partly decentralized multi-rate load alleviation controllers. In *ICAS 2022*. Stockholm, Sweden.

[10] Alam, M., Hromcik, M., and Hanis, T. (2015). Active gust load alleviation system for flexible aircraft: Mixed feedforward/feedback approach. *Aerospace Science and Technology*, 41, 122–133. doi: 10.1016/j.ast.2014.12.020.

[11] Fezans, N. and Joos, H.-D. (2017). Combined feedback and LIDAR-based feedforward active load alleviation. In *Proceedings of the 2017 AIAA Aviation Forum*. Denver, CO, USA. doi: 10.2514/6.2017-3548. AIAA 2017-3548.

[12] Wallace, C. and Fezans, N. (2023). Lidar-based gust load alleviation - results obtained on a generic long range aircraft configuration. In *Aerospace Europe Conference 2023*. Lausanne, Switzerland. doi: 10.13009/EUCASS2023-564.

[13] Hofstee, J., Kier, T., Cerulli, C., et al. (2003). A variable, fully flexible dynamic response tool for special investigations (VarLoads). In *IFASD 2003*. Amsterdam, Netherlands.

[14] Waszak, M. R. and Schmidt, D. K. (1988). Flight dynamics of aeroelastic vehicles. *Journal of Aircraft*, 25(6), 563–571. doi: 10.2514/3.45623.

[15] Bisplinghoff, R. L., Ashley, H., and Halfman, R. L. (1955). *Aeroelasticity*. Dover Publications Inc. ISBN 978-0486691893.

[16] European Union Aviation Safety Agency (EASA) (2021). *Certification Specifications and Acceptable Means of Compliance for Large Aeroplanes (CS-25) - Amendment 27*.

[17] Cavaliere, D., Fezans, N., Kiehn, D., et al. (2022). Gust load control design challenge including lidar wind measurements and based on the common research model. In *AIAA Scitech 2022 Forum*. San Diego, CA, USA. doi: 10.2514/6.2022-1934.

[18] Favre, C. (1994). Fly-by-wire for commercial aircraft: the airbus experience. *International Journal of Control*, 59(1), 139–157. doi: 10.1080/00207179408923072.

[19] Delannoy, S. and Oudin, S. (2013). Longitudinal control law for modern long range civil aircrafts. In *CEAS EuroGNC 2013*. Delft, The Netherlands.

[20] Puyou, G., Bérard, C., Ferreres, G., et al. (2006). Conception multi-objectif de lois de pilotage pour un avion de transport civil. *Journal Europeen des Systemes Automatises*, 40(1). doi: 10.3166/jesa.40.1019-1051.

[21] Sutherland, J. (1968). Fly-by-wire flight control systems. Tech. rep., Air Force Flight Dynamics Laboratory, Wright-Patterson Air Force Base, OH, USA. AD 679 158.

[22] Niedermeier, D. and Lambregts, A. (2012). Fly-by-wire augmented manual control - basic design considerations. In *ICAS 2012*. Brisbane, Australia.

[23] Fezans, N. (2017). An unusual structure for a feedforward gust load alleviation controller. In *CEAS EuroGNC 2017*. Warsaw, Poland. doi: 10.1007/978-3-319-65283-2. `https://elib.dlr.de/113998/`.

[24] Cavaliere, D. and Fezans, N. (2022). Recasting discrete 1-cosine gust requirements as frequency domain specifications for load alleviation control design. In *IFASD 2022*. Madrid, Spain. IFASD-2022-143.

[25] Padé, H. (1892). Sur la représentation approché d'une fonction par des fractions rationelles. *Annales Scientifiques de L'é.N.S.*, 9, 3–93. doi: 10.24033/asens.378.

[26] Cavaliere, D. and Fezans, N. (2024). Toward automated gust load alleviation control design via discrete gust impulse filters. *Journal of Guidance, Control, and Dynamics*, 47(4), 697–710. doi: 10.2514/1.G007762.

[27] Cavaliere, D. and Fezans, N. (2024). A practical approach to automated multiobjective gust load alleviation control design in a structured H_2/H_∞ framework. In *CEAS EuroGNC 2024*. Bristol, UK. CEAS-GNC-2024-042.

COPYRIGHT STATEMENT